RSC Advances

ROYAL SOCIETY OF CHEMISTRY

www.rsc.org/advances

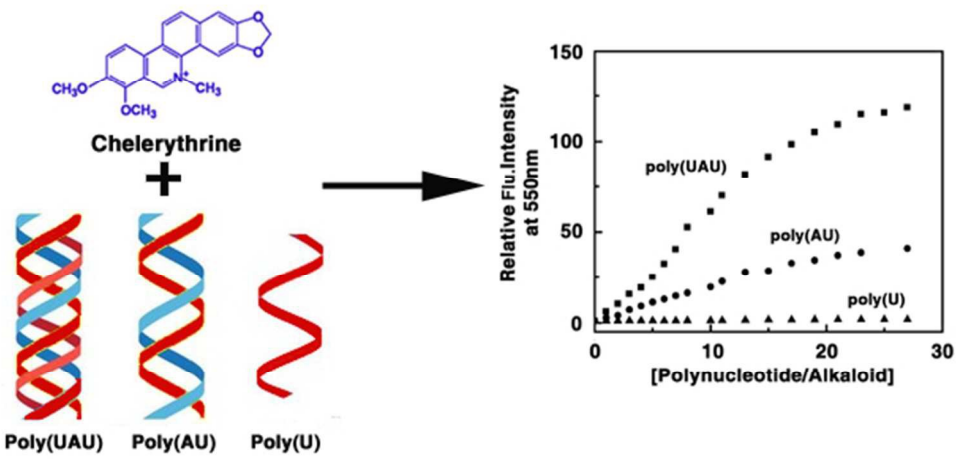

Interaction of CHL with poly(UAU), poly(AU) and poly (U)
223x108mm (72 x 72 DPI)

Structural and Thermodynamic Basis of Interaction of the Putative Anticancer Agent Chelerythrine with Single, Double and Triple-Stranded RNAs

Pritha Basu and Gopinatha Suresh Kumar*

Biophysical Chemistry Laboratory, Chemistry Division

CSIR-Indian Institute of Chemical Biology, Kolkata 700 032, India

Address for Correspondence

Prof. G. Suresh Kumar

Professor of Chemical and Biological Sciences and Senior Principal Scientist

Biophysical Chemistry Laboratory

CSIR-Indian Institute of Chemical Biology

4, Raja S. C. Mullick Road, Kolkata 700 032, INDIA

Phone: +91 33 2472 4049/2499 5723 ; Fax: +91 33 2473 0284

e-mail: gskumar@iicb.res.in/gsk.iicb@gmail.com

*To whom all correspondence should be addressed.

Abstract

A comparative study on the interaction of the natural plant alkaloid chelerythrine with triple helical poly(U)·poly(A)∗poly(U), double helical poly(A)·poly(U) and single stranded poly(U) (the dot and star representing the Watson-Crick and Hoogsteen base pairing) has been performed using various biophysical and thermodynamic techniques. Chelerythrine binds to the duplex and triplexes in a cooperative manner with affinity of the order 10^6 M^{-1}. A weaker binding (~10^5 M^{-1}) in a non-cooperative mode occurred with poly(U). Chelerythrine is more selective towards RNA triplex than its parent duplex. The triplex was stabilized specifically without affecting the stability of the duplex. Fluorescence quenching, fluorescence polarization, energy transfer from the nucleotides to the alkaloid, and viscosity results gave convincing evidence for a true intercalative binding of chelerythrine to the triplex and the duplex structures, and the partial base stacking with poly(U). The conformations of both double and triple helices were perturbed on binding but no effect occurred to the single strand structure. The binding of the alkaloid to all the three RNA helices was found to be exothermic; to the triplex it was entropy driven with favorable enthalpy change, to the duplex enthalpy driven and to the single strand it was enthalpy driven. These results provide new knowledge on the mode, mechanism and specificity, and energetics of binding of the natural alkaloid and putative anticancer agent chelerythrine to different RNA conformations.

Introduction

Advancement of the burgeoning new areas of genomics has unequivocally established the diverse and critical functions for RNA molecules in many cellular activities of the eukaryotic transcriptome.[1] Consequently, they have become important targets of small molecules and drugs for modulating therapeutic functions.[2-4] RNAs can exist in a multitude of structures and conformations that could be potential drug binding sites; they could also be either single, double stranded or triple helical structure.

A RNA triplex is an important tertiary structural motif that occurs in many pseudo knots. Double stranded RNA regions are the sites for triplex formation through sequence specific targeting and such opportunities are of great potential for a number of biological applications and therapeutic intervention.[5-13] The in vivo functions of triple-helical nucleic acids have been reviewed in considerable details recently.[14,15] Triplexes have low stability; the binding of the third strand to the duplex is weaker thermodynamically and slower kinetically. This is a critical limitation for their biological applications and hence it is required to develop small molecules with high affinity and selectivity that can selectively stabilize triple helical structures.[5,6,16] Double-stranded (ds) RNA's, on the other hand, are responsible for gene silencing and in inducing an antiviral defense status in human epidermal keratinocytes.[17] Noncoding microRNAs (mi RNAs) are processed from imperfect ds RNAs.[18-20] Double stranded sections of mRNA itself are often sites of interaction of proteins and small molecules.[21] Due to such importance of ds RNAs in cellular functions it has become a potential target for developing small molecule based therapeutics. Single stranded noncoding RNAs are also important for their versatile secondary structure and configuration which leads to the control of many cellular activities.

Chelerythrine (1,2-dimethoxy-12-methyl[1,3]benzodioxolo [5, 6-c] phenanthridinium chloride (C21H18ClNO4) CHL, Fig. 1),[22] is a benzophenanthridine alkaloid, is derived from the herb *Chelidonium majus* L. (Papaveraceae) plants.[23] A number of important biological applications of chelerythrine have been reported very recently, For example, it is a potent inhibitor of protein kinase C (PKC) responsible for the maintenance of erythrocyte deformability.[24-26] It also stimulates the production of reactive oxygen species, which may deplete cellular antioxidants, provide a signal for rapid execution of apoptosis,[27] and provoke cell death in a variety of tumour cells leading to potential application as an anticancer agent.[25,28-31] Chelerythrine inhibits BcL-XL function by displacing Bax binding, inducing apoptosis in several cancer cell lines.[28] Chelerythrine can activate p38 MAP kinase and JUNK signaling pathways, and induce apoptosis in cancer cells.[26,29] The DNA binding activity of chelerythrine was studied in details recently in our laboratory[32,33] to reveal that the binding occurs by intercalation with remarkable guanine-cytosine base pair specificity. A crystal structure data of chelerythrine-d(CGTACG)-complex at 2.10 A˚ is also available in the protein data bank.[34] The binding selectivity of chelerythrine to the biologically significant K^+-form of human telomeric DNA G-quadruplex and its binding specificity for human telomeric RNA G-quadruplex were established by the studies of Jiang and coworkers.[35] These results have proposed the alkaloid as a promising candidate for structure-based design and development of G-quadruplex specific ligands. The high binding of chelerythrine to poly(A) inducing self-structure was also reported very recently,[36] However, no studies with double and triple stranded RNAs are reported till now. A structurally

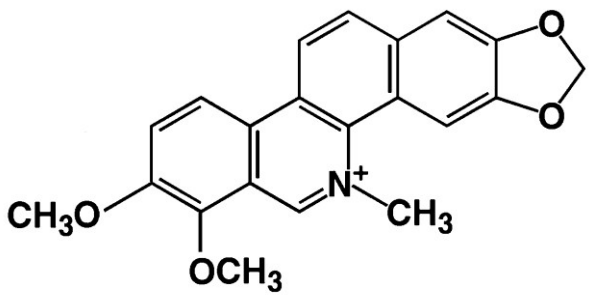

Fig. 1

Fig. 1. Molecular structure of iminium form of CHL.

similar alkaloid, sanguinarine is reported to bind to duplex and triplex RNAs.[37] Since the importance of chelerythrine has been exemplified in many very recent studies as mentioned above and being a natural product with the advantage of less toxic and wide natural abundance we felt the necessity to examine its potential in stabilizing the triplex structure. Here we characterized its binding to poly(U)·poly(A)*poly(U) (hereafter poly(UAU) triplex in comparison with the parent double helical poly(A)·poly(U) (hereafter poly(AU)) and to the single stranded poly(U) using spectroscopic and calorimetric techniques.

Results and discussion

Formation of triple helical RNA

RNA triplex, poly(UAU), was prepared by the method described in the material and methods section. The formation of the triplex was confirmed from its biphasic melting profile and typical circular dichroism (CD) spectral pattern.[37,38] In the optical melting profile the first T_m (T_{m1}) was at 36 °C followed by the second T_m (T_{m2}) at 47 °C. The characteristic biphasic melting transition in this triplex with the second transition temperature corresponding to that observed for the melting of the parent duplex poly(AU) clearly indicated the formation of a stable triple helical structure, and these were in conformity with literature reports.[37,38] The intrinsic CD spectral pattern of the triplex was found to be significantly different from that of the duplex spectrum with lower ellipticity values for the peaks of the triplex[38] again confirming the formation of the triplex. Once the triplex formation was confirmed we sought to characterize the interaction.

Binding equilibria: absorbance and fluorescence spectral studies

The binding equilibrium of CHL to the poly(UAU), poly(AU) and poly(U) can be represented by the following equation

$$[P] + [D] \longrightarrow [PD] \qquad (1)$$

Here [P] denotes the equilibrium concentration of the RNA helices and the [D] denotes equilibrium concentration of CHL. [PD] denotes the equilibrium concentration of the RNA-CHL complex.

CHL has a typical absorption spectral pattern in the 300–600 nm regions with a maximum around 316 nm (see curve 1 in Fig. 2), the change in which was used to monitor the interaction phenomenon. Absorbance spectral titration profiles of CHL in the presence of increasing concentrations of the three RNA's are depicted in Fig. 2. Strong hypochromic and bathochromic effects were visible in the absorption bands of the alkaloid in the presence of incremental amounts of poly(UAU) and poly(AU) (Fig. 2A, B). On the other hand, smaller hypochromic effect and bathochromic shift were observed in the presence of poly(U) (Fig. 2C). The 316 nm

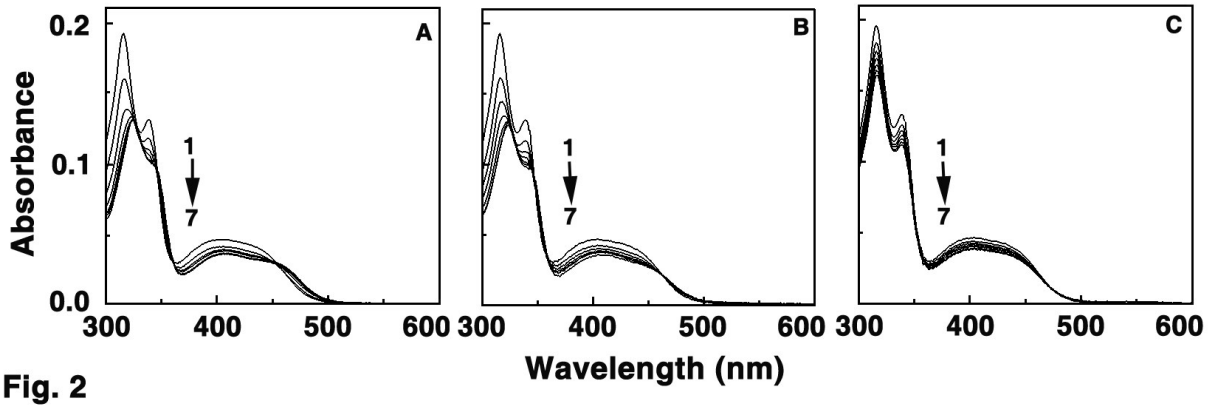

Fig. 2

Fig. 2. Absorption spectra of CHL (4 µM) treated with increasing concentrations of (A) poly(UAU) in the range 0-40 µM, (B) poly(AU) in the range 0-48 µM and (C) poly(U) in the range 0-80 µM represented by curves (1-7). in each case.

band of the alkaloid spectrum was red shifted by 9, 6 and 1 nm, respectively, in the presence of poly(UAU), poly(AU) and poly(U); the absorbance decreased concomitantly by 33%, 30%, and 18%, respectively. Such spectral changes, particularly for the triplex and the duplex, may be attributed to arise due to strong interaction between the π electron cloud of the aromatic chromophore of the alkaloid and the RNA helices, most likely due to intercalation. The presence

of isosbestic points at 358 and 461 nm, respectively, indicated the formation of a single type of complex over the input concentration range of the RNAs. This indicated strong intermolecular association between the alkaloid and the triplex and the duplex.

Evidence for the association of CHL to these RNA helices was also derived from fluorescence spectral titration data. The spectral titration profiles of CHL with the RNA's are presented in Fig. 3A-C. It can be seen that the weak intrinsic steady state fluorescence of CHL in the range 450–650 nm enhanced remarkably upon complexation with poly(UAU) and poly(AU), but very little change was observed for poly(U) even at very high concentrations. This strong enhancement of the fluorescence intensity suggested an effective interaction of the electronic cloud of the bound alkaloid molecules and the nucleotides consequent to strong binding. Enhancement in the

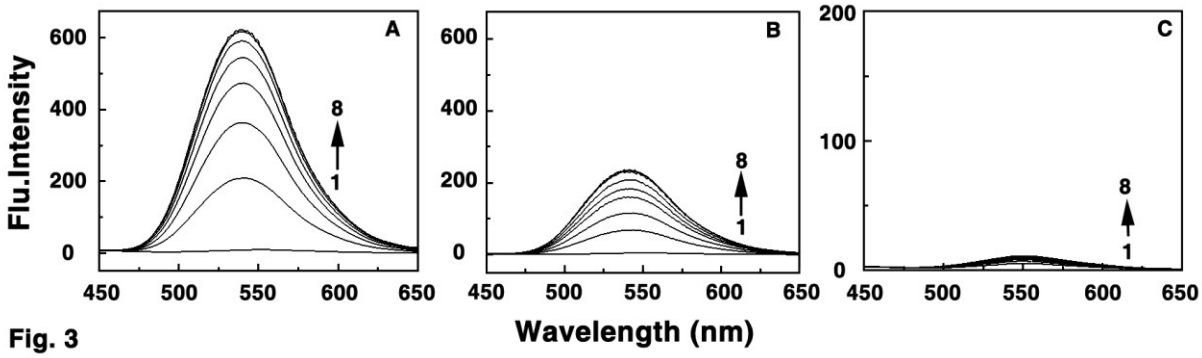

Fig. 3

Fig. 3. Fluorescence spectral titration of CHL (2 μM) with increasing concentration of (A) poly(UAU) in the range 0-52 μM, (B) poly(AU) in the range 0-100 μM, and (C) poly(U) in the range 0-200 μM as represented by curves (1-8) in each case.

presence of poly(UAU) was much higher than with the other systems indicating that the strongest binding occurred with the triplex suggesting the presence of the bound alkaloid in more hydrophobic and constrained region of triplex than the duplex and single stranded structures; this again reflecting the higher association of CHL to poly(UAU) than poly(AU) and poly(U). From the fluorescence titration study we can interpret that CHL binds strongly with triplex and duplex and with single stranded RNA the interaction was very weak. Therefore, CHL shows selectivity

towards poly(UAU) over poly(AU) and poly(U). This result corroborated the spectral changes observed in absorbance titration.

Analysis of the spectral titration data and estimation of the binding parameters

The presence of sharp isosbestic points in the absorption titration data indicated the prevalence of equilibrium binding conditions. Therefore, the amount of free (C_f) and bound alkaloid (C_b) at each step of the spectral titration was determined performing a reverse titration in absorbance and fluorescence as described in details previously.[39,40] Binding data obtained from the absorbance and fluorescence titrations were then cast into Scatchard plots of r/C_f versus r. The plots are presented in Fig. S1.

The Scatchard plots of poly(UAU) and poly(AU) reveal positive slope at low binding ratios characteristic of cooperative binding isotherms.[40] Therefore, the plots were analyzed using the McGhee–von Hippel equation (*vide infra*) for cooperative binding[41]as described in details previously.[39,40] On the other hand, a negative slope in the plot observed for poly(U) at low binding ratios is characteristic of non cooperative[42] and the plot was analyzed by McGhee–von Hippel equation for non-cooperative binding.[41] The binding affinity values obtained from the analysis are presented in Table 1. It can be seen that a relatively higher affinity was observed for the poly(UAU) triplex over the duplex. The apparent binding constants (K_ω), which is a product of K_i and ω from the absorption data gave values of $1.69 \pm 0.021 \times 10^6$ and $1.45 \pm 0.081 \times 10^6$ M^{-1}, respectively, for poly(UAU) and poly(AU), and the value of intrinsic binding constant K_i was $2.73 \pm 0.062 \times 10^5$ M^{-1} for poly(U). Similarly, from the fluorescence data we obtained the apparent binding constants as $1.68 \pm 0.020 \times 10^6$ and $1.43 \pm 0.051 \times 10^6$ M^{-1}, respectively, for poly(UAU) and poly(AU) and K_i for poly(U) was $2.64 \pm 0.051 \times 10^5$ M^{-1}. The number of excluded sites (n) consequent to the binding of a single alkaloid is lowest for the triplex and were higher

TABLE 1

Binding parameters for the complexation of CHL with RNA evaluated from Scatchard plots analyzed by the McGhee-von Hippel analysis of the absorbance and fluorescence titration data[a].

Method	System	$K_i \times 10^{-5}$ (M^{-1})[b]	n	ω	$K\omega \times 10^{-6}(M^{-1})$
Absorbance	CHL+poly(UAU)	1.003 ± 0.015	3.95±0.012	16.88 ± 0.220	1.69 ± 0.021
	CHL + poly(AU)	0.718 ± 0.017	4.48±0.013	20.14±0.561	1.45 ± 0.081
	CHL+ poly(U)	2.726 ± 0.062	5.43±0.090	–	–
Fluorescence	CHL+poly(UAU)	0.998 ± 0.009	4.13±0.008	16.84 ± 0.226	1.68 ± 0.020
	CHL+poly(AU)	0.727 ± 0.016	4.54±0.010	19.68 ± 0.568	1.43 ± 0.051
	CHL+poly(U)	2.635 ± 0.051	5.42 ± 0.10	–	–

[a]Average of four determinations. [b]Binding constants (K_i) and the number of binding sites (n) refer to solution conditions of sodium cacodylate buffer, pH 6.3. ω is the cooperativity factor. The values given above are averages of four determinations.

for duplex and single strands. The values clearly suggest the higher affinity of the alkaloid to the triplex over duplex conformation. On the other hand, the binding to the single strand is much weaker than those with the duplex and the triplex. It is likely that the alkaloid is able to intercalate to both the triplex and duplex and only stack with the single strand and this causes the marked difference in the binding affinity values.

Binding stoichiometry determination

Having determined the affinity of CHL to the three RNA conformations we determined the stoichiometry of binding of CHL to the triplex, duplex and the single stranded RNA from the continuous variation analysis procedure (Job plot).[37,39] The Job plots depicting the differences in the fluorescence intensity versus mol fraction of CHL revealed a single binding mode in each

case. From the inflection points, $\chi_{alkaloid}$ = 0.20, 0.19, 0.17, respectively, for poly(UAU), poly(AU) and poly(U) the corresponding site sizes were estimated to be 3.99, 4.19, 4.86, respectively, for the complexation of CHL (Fig. S2). The trend and magnitude of these values are more or less similar to the number of excluded sites evaluated from the McGhee-von Hippel analysis of the spectral data.

Fluorescence polarization anisotropy

Additional support for the strong association of CHL to the RNA's was obtained from fluorescence polarization studies. Polarization results may also be used to infer the mode of

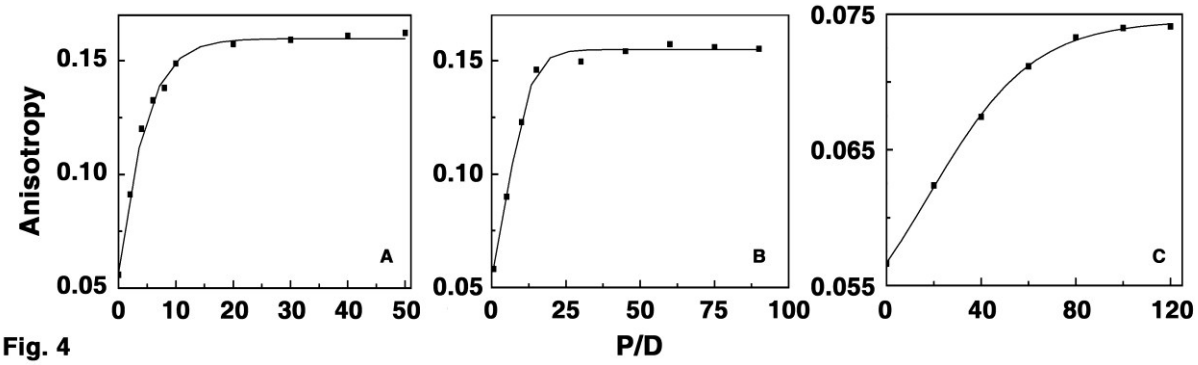

Fig. 4

Fig. 4. Change of fluorescence anisotropy of CHL on binding with (A) poly(UAU), (B) poly(AU), and (C) poly(U).All the data in this plot are determined from the fluorescence anisotropy experiments. The data points are the mean of four determinations.

binding of CHL to the RNA's. The basis of this technique to monitor molecular interactions lies on the fact that larger molecules tumble slowly than the smaller molecules. Polarization results can suggest the probable location of the small molecules in heterogeneous environment of RNA. Binding of the alkaloid reduces its mobility resulting in an increase of its anisotropy in the bound form. The value of 0.056 evaluated for the free CHL increased to 0.162, 0.155 and 0.074, respectively, on binding with poly(UAU), poly(AU) and poly(U) (Fig. 4). The highest anisotropy value for poly(UAU) indicated the relative stronger association of CHL with poly(UAU)

compared to poly(AU) and poly(U). This data provided insight on the strong interaction of the alkaloid on one hand and likely intercalation to poly(UAU) and poly(AU) helices, on the other. The low value with poly(U) is indicating the inability of the alkaloid to intercalate with this structure. Further studies like fluorescence quenching and viscosity measurements were performed to illustrate the mode of binding.

Fluorescence quenching studies by iodide ions

The degree of fluorescence quenching by anionic quenchers is a simple method of investigating the mode of binding of a small molecule to nucleic acids. The theory is that the molecules bound to the surface of the macromolecule by electrostatic interaction or in the grooves may be easily accessible to the quencher while those bound inside the helix in an intercalative mode are inaccessible. In particular, anionic quenchers like I^- cannot access the inside of the helix due to the strong electrostatic repulsion from the negatively charged phosphate groups and consequently very little quenching will be observed for those molecules intercalated. So, the magnitude of the Stern–Volmer quenching constant (K_{sv}) of CHL if buried inside by intercalation will be lower than that of the free molecules in the presence of I^-. Here, the K_{sv} value of free CHL was 65 M^{-1} while the values for those bound to poly(UAU), poly(AU) and poly(U) were 10, 23 and 45 M^{-1}, respectively (Fig. 5A). This suggests that the CHL molecules bound to both the triplex and duplex RNAs were sequestered away from the solvent, while those bound to the single stranded RNA were largely accessible to I^-. This result suggests an intercalation mode for CHL binding to poly(UAU) and poly(AU), and an external binding or stacking mode with poly(U).

Viscosity results: Evidence for intercalation

To further prove the intercalation of CHL to the triplex and duplex structures we performed viscosity studies. Intercalation of a small molecule between the base pairs of duplex DNA and RNA has been shown to result in an increase in viscosity due to ligand-induced lengthening of the helix.[43] Figure 5B illustrates the effect of CHL on the viscosity of rod like form of duplex and triplex RNA. The total increase in viscosity and shape of the curve for triplex is similar to those observed for the parent duplex inferring the intercalation mode of binding with both poly(UAU) and poly(AU). The net increase of helix length for the triplex was, however, less than that with the duplex; this may happen as the nature of the intercalative binding to the triple helix may lead to a smaller increase in helix length per bound ligand than that observed for the duplex. Scaria and Shafer had observed a smaller viscosity change for ethidium-poly(dA).2poly(dT) compared to its parent duplex.[44] It was suggested that the presence of a third strand in the minor groove and the likely hood that the base triplets (triplex) may not be perpendicular to the helix axis like the

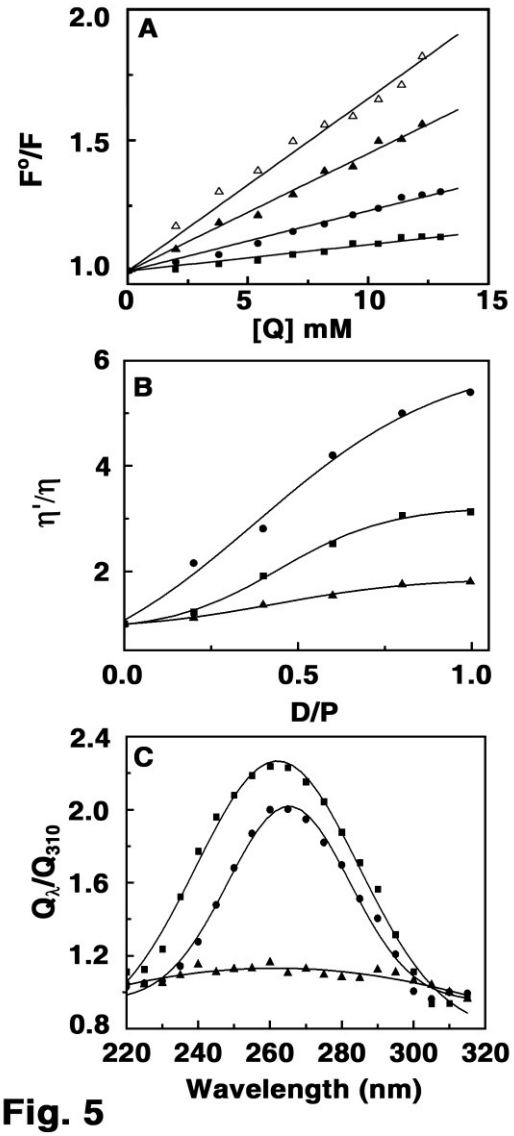

Fig. 5

Fig. 5. (A) Stern-Volmer plots for the quenching of free CHL (Δ) and complexes with poly(UAU) (■), poly(AU) (●) and poly(U) (▲), (B) A plot of variation of the (η′/η) with varying molar ratio for the complexation of the CHL to poly(UAU) (■), poly(AU) (●) and poly(U) (▲), and (C) variation of relative quantum yield of CHL in the presence of poly(UAU) (■), poly(AU) (●) and poly(U) (▲).All the data in this plot are determined from the average of four determinations.

base pairs (duplex) may result in to a smaller helix lengthening on intercalation to a triplex compared to duplex. So also if the triplex form contained other structures like branched, structures, the viscosity may not be very sensitive to length changes in the presence of ligands as suggested by Scaria and Shafer[44] For single stranded RNA no significant change was observed in the viscosity confirming lack of intercalation of CHL in poly(U).

Fluorescence energy transfer: Additional evidence for intercalation

Although viscosity results have proved intercalation we sought to obtain additional evidences for the mode of binding. Le Pecq and coworkers,[45-47] had shown that fluorescence energy transfer can occur from DNA/RNA to bound drugs leading to an increase in the fluorescence quantum yield in the wavelength range corresponding to the DNA/RNA absorbance; this may be used as additional evidence for intercalative binding as efficient energy transfer is possible only if the bound drug is in close contact with, and oriented parallel to the base/base pairs and base triplets. Figure 5C shows the plots of the ratio Q_λ/Q_{310} against wavelength for the duplex, triplex and the single stranded RNAs. It can be seen that both the duplex and the triplex lead to an increase in quantum yield but poly(U) effects almost no increase. Furthermore, the increase in quantum yield for the triplex is much higher than that for the duplex. This provides strong evidence for intercalative binding of CHL to both triplex poly(UAU) and duplex poly(AU)on one hand and reveals that binding to the triplex form to result in substantially higher energy transfer compared to the duplex on the other leading to higher selectivity to the triplex over the duplex.

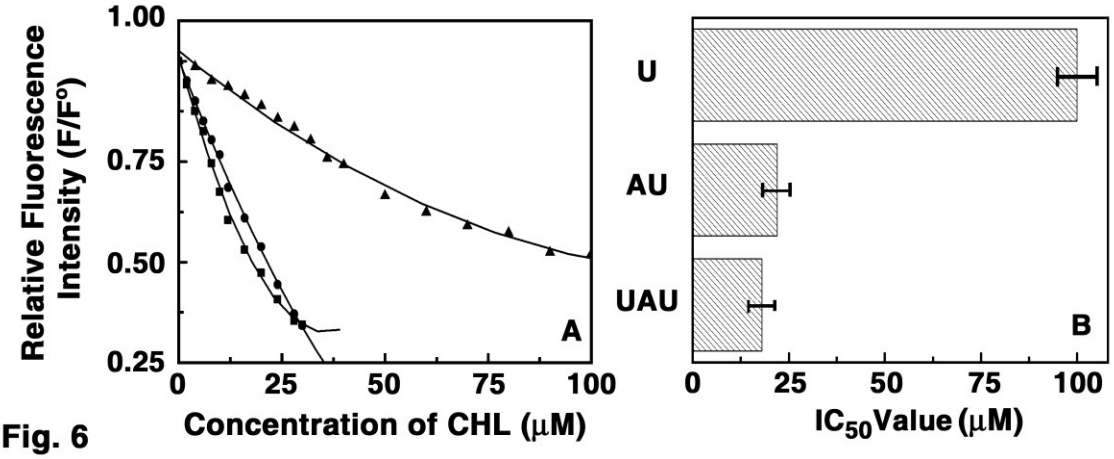

Fig. 6

Fig. 6 (A) Relative fluorescence intensity decrease of EtBr (7 μM)-poly(UAU) (■), poly(AU) (●) and poly(U) (▲) (50 μM) complex induced by the binding of CHL conducted in 50 mM Tris HCl buffer (pH 6.3). (B) The values of IC_{50} of poly(UAU), poly(AU) and poly(U) are shown as a bar graph.

Ethidium bromide displacement assay

In another method to ascertain the binding mode we performed ethidium bromide **(**EtBr) displacement assay by fluorescence titration. EtBr is a well known intercalator to DNA/RNA[48] and the fluorescence of the nucleic acid intercalated EtBr is enhanced many fold. Displacement of EtBr from the intercalated sites is expected to decrease the fluorescence and hence may serve as a sensitive probe to infer on the intercalation properties of CHL. The data presented in Fig. 6A clearly showed that CHL quenched the fluorescence intensity of EtBr –RNA complexes. The result reveal that CHL can displace EtBr easily from its complex with poly(UAU) and poly(AU). In the case of poly(U), under the identical conditions, very high concentration of CHL was needed to quench 50% fluorescence intensity. IC_{50} values of CHL for different RNA systems are presented in Fig. 6B as a bar diagram. From the results we can infer the interactive binding mode of CHL with poly(UAU) and poly(AU).

Spectroscopic study using circular dichroism: Conformational aspects

Circular dichroism (CD) spectroscopy was employed to probe the conformational aspects of the complexation. The CD spectra were recorded in the 210–400 nm regions. The CD spectrum of the triplex exhibited a positive band at 263 nm and an adjacent negative peak at 242 nm followed

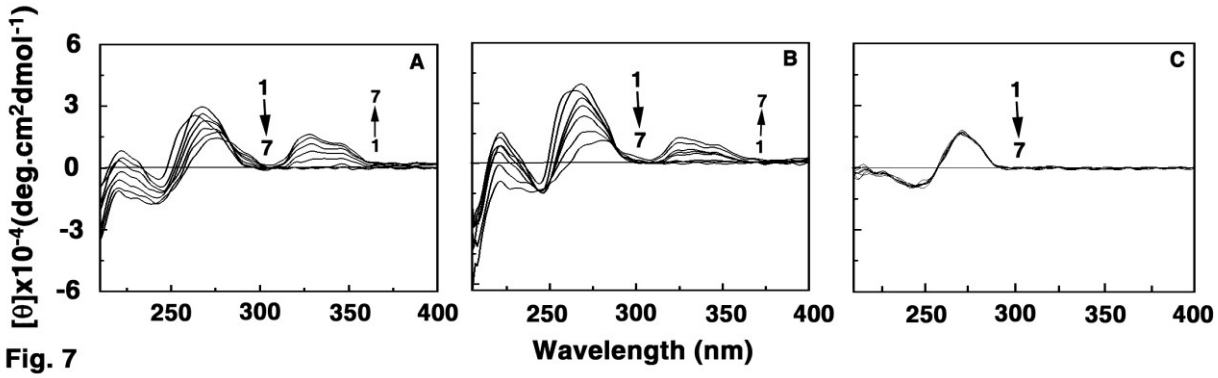

Fig. 7. Circular dichroism spectral changes of (A) poly(UAU) (30 µM), (B) poly(AU) (30 µM), and (C) poly(U) (30 µM) on interaction with increasing concentration of CHL in the range of 0-30 µM.

by a small positive band at 223 nm (Fig. 7A). These bands emanate from the stacking interactions between the base triplets and the helical structure of the triplex strands.[37,42] In the case of poly(UAU)-CHL interaction, a red shift in the wavelength maximum of the 264 nm band followed by concomitant decrease of the ellipticity and a strong induced CD signal observed in the range of 300-400nm with a maxima of 357nm. The RNA duplex exhibited a gross A-conformation with a large positive band around 267 nm (Fig. 7B). Binding of CHL slightly red shifted and decreased the long wavelength positive band ellipticity and an induced CD signal was observed in 300-400 nm range as the interaction progressed. Poly(U) has characteristic positive band at 268 nm but no CD changes were observed in the presence of CHL and no induced CD signals were observed in 300-400 nm range. These results further substantiate the interaction of CHL with both duplex and triplex, which leads to the change in their conformation and essentially weak interaction with poly(U) resulting in little conformational changes.

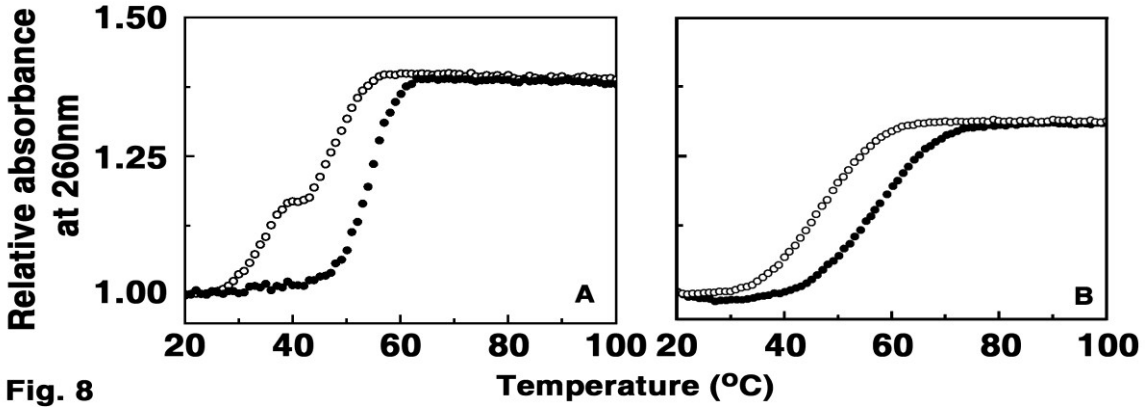

Fig. 8

Fig. 8. Optical melting profiles of (A) poly(UAU) (○) and poly(UAU)-CHL complex at saturating D/P ratio (●), (B) poly(AU) (○) and poly(AU)-CHL complex at saturating D/P ratio (●).

Optical melting and differential scanning calorimetry studies

The optical melting experiment is an important tool to investigate the interaction of small molecules to nucleic acid duplexes and triplexes. It is particularly informative in triplexes as the effect on third strand can be observed in comparison to the effect on the duplex. An enhancement in the melting temperature may be the net effect of neutralization of the phosphate charges through binding and strong stacking interactions of the intercalated molecules. Optical melting profiles of the poly(UAU) and its complexes with CHL at saturated D/P (alkaloid/polynucleotide molar ratio) values are shown in Fig. 8A. Under the conditions of the present experiment the third strand denaturation (triplex to duplex) occurred at 36.0 ^{o}C and the duplex denaturation (duplex to single strands) occurred at 47.2 ^{o}C. The quantitative data on the melting temperature of the poly(UAU) triplex and its complex with CHL is presented in Table 2. A ΔT_m value of 18^{o}C was obtained under helix saturating conditions with the triplex.

The melting profiles of RNA duplex poly(AU) on complexation with CHL is presented in Fig. 8B. The T_m value for poly(AU) was 46.6 ^{o}C. The binding of CHL strongly stabilized poly(AU) enhancing the melting temperature by 10.1 ^{o}C under saturating conditions. The result clearly indicates that CHL stabilized poly(UAU) much more than poly(AU), which reflects the specificity of CHL to the poly(UAU) over poly(AU). No melting profile was observed for poly(U) and the presence of the alkaloid effected no change in the pattern of the profile (not shown).

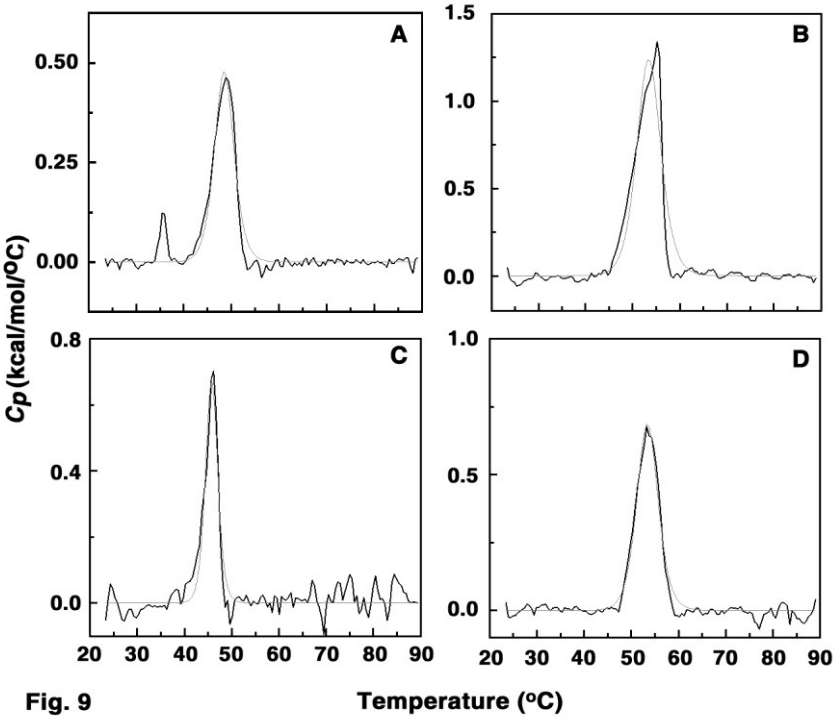

Fig. 9. DSC profiles of (A) only poly(UAU), (B) poly(UAU)-CHL complex at saturating D/P, (C) only poly(AU) and (D) poly(AU)-CHL complex at saturating D/P ratio.

To study the thermal stabilization, differential scanning calorimetry **(**DSC) experiments were also performed. DSC studies of CHL–RNA complexes presented in Fig. 9A-D also revealed similar stabilization temperature as observed in optical melting presented in Table 2. DSC profiles of both the bound and unbound nucleotides thus confirm stabilization of the duplex and triplex on alkaloid binding.

TABLE 2

UV and DSC melting temperatures of RNAs and RNAs-alkaloid complex[a]

Methods	System	D/P	T_m (°C) 3→2	T_m (°C) 2→1	ΔT_m(°C) 3→2	ΔT_m (°C) 2→1
UV Optical Melting	poly(UAU)	0	36.00	47.20	-	-
	poly(UAU) +CHL	0.4	53.90	-	17.90	-
	poly(AU)	0	-	46.60	-	-
	poly(AU)+CHL	0.8	-	56.70	-	10.10
DSC	poly(UAU)	0	35.50	47.4		
	poly(UAU) +CHL	0.4	53.48		17.98	
	poly(AU)	0	-	45.75	-	-
	poly(AU)+CHL	0.8	-	54.41	-	8.66

[a] Average from three experiments. T_m (°C)3→2 and T_m (°C)2→1 correspond to triplex to duplex and duplex to single strand transitions, respectively. $\Delta T_m = T_m$ of RNA-alkaloid complex - T_m of RNA.

Thermodynamic characterization of CHL–RNA interaction: Isothermal titration calorimetry

To understand the thermodynamics of the interaction of CHL with triplex, duplex and single stranded RNA, detailed thermodynamic data were gathered from high sensitive isothermal titration calorimetric (ITC) studies. ITC measurements provide detailed information[49,50] on energetics with data on standard molar enthalpy of binding, the entropy contribution to the binding, standard molar Gibbs energy, and also the affinity and stoichiometry of the interaction. We also obtain the binding affinity directly. In Fig. 10 representative calorimetric profiles of the titration of CHL to poly(UAU), poly(AU) and poly(U) at 20 °C are presented. The binding is an exothermic process and has a single binding event in all the three cases. The binding affinity (K_a)

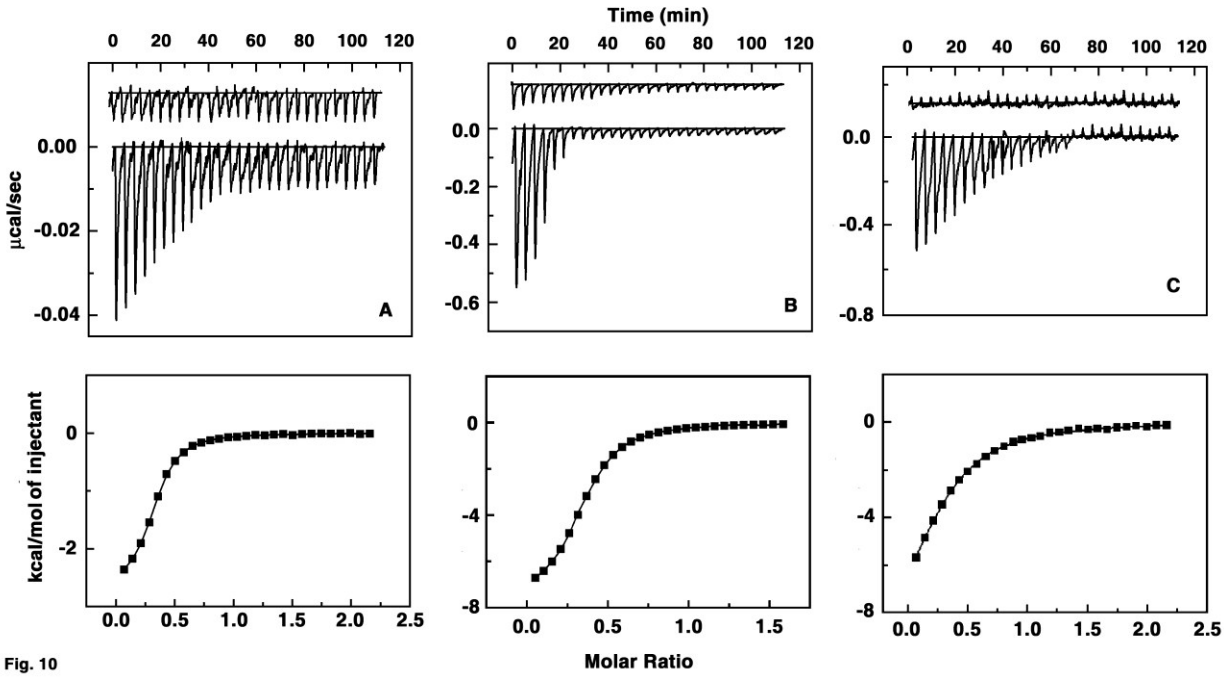

Fig. 10

Fig. 10. ITC profiles for the titration of CHL with (A) poly(UAU), (B) poly(AU), and (C) poly(U) at 20 °C in sodium cacodylate buffer at pH 6.3. The top panels represent the raw data resulting from the sequential injection of RNAs into polynucleotide solutions and the lower panels represent the corresponding normalized heat signals versus molar ratio. The data points (■) are the experimental injection heats while the continuous line is the best fit to the experimental data.

values obtained from ITC are of the order of 10^6 M^{-1} for the triplex and duplex, and of the order of low 10^5 for poly(U). The binding affinity of the CHL to poly(UAU), poly(AU), and poly(U) at 20 °C was estimated to be 1.77×10^6, 1.51×10^6 and 2.81×10^5 M^{-1}, respectively. The site size (n) values, the reciprocal of the stoichiometry N, were found to be 3.1, 2.9 and 3.4, respectively, for CHL binding to poly(UAU), poly(AU) and poly(U). These values are presented in Table 3. The binding affinity values follow the same trend as those obtained from spectroscopic studies, being highest for the poly(UAU) and varying in the order poly(UAU) > poly(AU) > poly(U) helices. The binding to poly(UAU) was driven largely by positive entropy and a negative enthalpy changes. With poly(AU) the binding was favored by enthalpic contributions, and in the case of poly(U) the binding was favored by large negative enthalpy change and unfavorable

entropy change. The thermodynamic parameters are listed in Table 3. An analysis of the data enables us to conclude that the CHL offered more favorable contacts with the bases of the triplex thereby accounting for the enhanced binding preference. The strong positive entropic term is apparently due to the disruption and release of structured water molecules from the triple helix upon intercalation of CHL.[51-53] Therefore, not only a significant increase in the binding affinity was observed but there were remarkable shifts in the energetics of the complexation as well in the complexation of CHL with these structures. CHL also shows high affinity to the duplex which may account for the strong enthaplic and entropic terms and it shows relatively low affinity towards the single stranded poly(U).

TABLE 3

Thermodynamic parameters for the association of CHL with poly(UAU), poly(AU) and poly(U) from isothermal titration calorimetry.

RNA conformation	$K_a \times 10^{-6}$ (M^{-1})	n	ΔG^o (kcal/mol)	ΔH^o (kcal/mol)	$T\Delta S^o$ (kcal/mol)
poly(UAU)	1.77±0.04	3.1	-8.39±0.02	-2.70±0.02	5.69±0.01
poly(AU)	1.51±0.03	2.9	-8.28±0.04	-7.69±0.01	0.59±0.02
poly(U)	0.28±0.01	3.4	-7.32±0.05	-10.92±0.05	-3.60±0.01

All the data in this table are derived from ITC experiments conducted in sodium cacodylate buffer at pH 6.3 at 20 ^oC and are average of four determinations. K_a and ΔH^o values were determined from ITC profiles fitting to Origin 7.0 software as described in the text. The values of ΔG^o were determined using the equation $\Delta G^o = \Delta H^o - T\Delta S^o$. n is site size which is reciprocal to N, the binding stoichiometry. All the ITC profiles were fit to a model of single binding site.

Comparison of chelerythrine binding with sanguinarine

Chelerythrine has close structural similarity to sanguinarine. It is therefore relevant here to compare the binding of these two compounds with poly(UAU) and to the AU. The binding of

sanguinarine to the triplex and duplex RNA was reported to be by non cooperative binding. This is in contrast to the cooperative binding observed here for chelerythrine. The stabilization of the triplex by chelerythrine was higher by about 3^{o}C compared to sanguinarine suggesting a better selectivity for chelerythrine to the triplex. Again, chelerythrine stabilized the duplex (10^{o}C) lower than the stabilization induced by sanguinarine (11.5^{o}C).[37] Furthermore, sanguinarine binding stabilized both the third strand and the duplex while chelertythrine stabilized only the triplx. In addition, the conformational changes induced by chelerythrine top the triplex were much stronger than that effected by sanguinarine. The thermodynamics of the interaction of the two compounds were also distinctly different. While the standard molar Gibbs energy changes for the interaction of both compounds were comparable, the contributions of the enthalpy and entropy terms to ΔG^{o} were distinctly different. Sanguinarine binding was favored by very high negative enthalpy contribution while that of chelerythrine was favored by similar higher entropy term. Therefore, it follows that although both compounds have closely similar chemical structure, chelerythrine bound and stabilized the triplex structure much effectively than sanguinarine.

Conclusions

In this study we investigated the binding aspects of chelerythrine with RNA triplex poly(UAU) in comparison with the duplex poly(AU) and single stranded poly(U). The following conclusions emerge from the results presented above. Chelerythrine binds in a similar way with triplex RNA as it does with duplex RNA, acting as an intercalating agent. The alkaloid binds and stabilizes the triplex structure selectively without effecting the duplex counterpart leading to its potential use as a triplex stabilizing agent. Although structurally closer, there are significant differences in the energetics of the interaction; being favored by both enthalpy and entropy changes compared

to the enthalpy driven binding to the duplex. The study suggest that in spite of a large amount of existing data that is available and for the prediction of a small molecule binding to duplex or triplex a convincing understanding is possible only on actually performing the experiments. In summary, these findings provide new insights on alkaloid-RNA interactions which may enable the development of more potent alkaloid based therapeutic agents.

Materials and methods

Materials

Chelerythrine chloride (CHL) (CAS No. 3895-92-9, purity > 95%), poly(U).poly(A) and poly(U)) were purchased from Sigma-Aldrich LLC (St. Louis, MO, USA) and used as obtained. Concentrations of poly(AU) and poly(U) were determined using known molar absorption coefficient (ε) values.[39,54] CHL concentration was determined by absorbance measurements using ε value of 37,060 M^{-1} cm^{-1} at 316 nm.[55] CHL was twice recrystallised from alcohol and dried in a desiccator at 40^{o}C. All experiments were conducted in 10 mM sodium cacodylate buffer containing 25 mM NaCl and 0.1 mM Na_2EDTA, at pH 6.3 (total Na^+ concentration = 35 mM) at 20^{o}C unless otherwise specified.

Preparation of the RNA triplex poly(UAU)

Poly(UAU) triple helix was prepared by mixing single stranded poly(U) and duplex poly(AU) in equimolar ratio in the aforementioned buffer, heating to 95^{o}C on a peltier controlled heating device, and then cooling slowly at a rate of 0.5 ^{o}C min^{-1} to 5 ^{o}C as reported earlier.[42] Circular dichroism spectral pattern and the biphasic optical melting profile confirmed the formation of the triple helical structure.[37,38,42]

Methods

Absorption and fluorescence spectral studies and elucidation of the binding parameters

Absorbance studies were done on Jasco V 660 spectrophotometer (Jasco International Co. Ltd., Hachioji, Japan) at 20 ± 0.5 ^{o}C equipped with a thermoelectrically controlled cell holder and temperature controller in matched quartz cuvettes of 1 cm path length (Starna cells, USA) using the methodologies described in details earlier.[56] Steady state fluorescence measurements were performed on a Shimadzu RF-5301PC spectrofluorimeter (Shimadzu Corporation, Kyoto, Japan) in fluorescence free quartz cuvettes of 1 cm path length as described previously.[56] The excitation wavelength of CHL was at fixed at 338 nm and the emission spectra was monitored in the range of 450-650 nm.[57] All the measurements were performed keeping an excitation and emission band pass of 5 nm at 20 ± 1.0 ^{o}C.

The amount of free and bound alkaloid was determined as follows. In absorption spectroscopy, after each addition of the alkaloid to the RNA solution from the absorbance value at the isosbestic points (A_{iso}) the total alkaloid concentration present was calculated as C_t=A_{iso}/$l\varepsilon_{iso}$. Here l is the path length of the cuvette and ε_{iso} is the molar absorption coefficient at the isosbestic point. The expected absorbance at the λ_{max} was calculated as A_{exp} = $lC_t\varepsilon_{max}$, where ε_{max} is the molar absorption coefficient at the λ_{max}. The difference of A_{exp} and the observed absorbance (A_{obsd}) yielded the calculated the amount of bound alkaloid as C_b = $\Delta A/1\Delta\varepsilon$ = (A_{exp} - A_{obsd})/l(ε_f - ε_b). Once C_b is known the free alkaloid concentration was determined as, C_f = C_t - C_b. The molar absorption coefficient of the completely bound alkaloid was estimated by adding a known quantity of the alkaloid to a large excess of RNA as, ε_b = A_{max}/lC_t. In fluorescence spectroscopy C_b was calculated using the relation C_b=C_t (I - I_o) / (V_o - 1)I_o, where C_t is the known total alkaloid concentration, I is the observed fluorescence, I_o is the fluorescence intensity of identical

concentration of alkaloid in absence of RNA and V_o is the experimentally determined ratio of the fluorescence intensity of the fully bound alkaloid to that of the free alkaloid. Free alkaloid concentrations (C_f) in both absorbance and fluorescence were obtained from the relationship $C_t = C_b + C_f$. The binding ratio r is obtained as the ratio of C_b / $[RNA]_{total}$.

The data obtained from absorbance and fluorescence titrations were cast into Scatchard plots of r/C_f versus r. The Scatchard isotherms with positive slope at low binding ratios (r) were analyzed using the following McGhee–von Hippel equation for cooperative analysis using equation.[41]

$$\frac{r}{C_f} = K_i(1-nr)\times\left(\frac{(2\omega+1)(1-nr)+(r-R)}{2(\omega-1)(1-nr)}\right)^{(n-1)}\left(\frac{1-(n+1)r+R}{2(1-nr)}\right)^{2} \qquad (2)$$

where $$R = \{[1-(n+1)r]^2 + 4\omega r(1-nr)\}^{\frac{1}{2}}$$

Here K_i is the intrinsic binding constant to an isolated alkaloid binding site on RNA, 'n' is the binding site size of a single alkaloid molecule, and ω is the cooperativity factor. The binding data were analyzed using Origin 7.0 software to determine the best-fit parameters of K_i 'n' and ω to equation (1).The isotherm with negative slope was analyzed by the non-cooperative binding model of McGhee and von Hippel. [41]

$$r/C_f = K_i\,(1\text{-}nr)[(1\text{-}nr)/\{1\text{-}(n\text{-}1)r\}]^{(n\text{-}1)} \qquad (3)$$

All the binding data were analyzed using Origin 7.0 software (Microcal Inc., Northampton, MA, USA) to determine the best-fit parameters of *K*i and n as described in details elsewhere. [39,42,58]

Determination of the binding stoichiometry

The binding stoichiometry was determined by using the continuous variation method of Job from the fluorescence spectral data.[59] The fluorescence intensity of the alkaloid-RNA complex at 550 nm was recorded keeping the total molar concentration of the two binding partners, the alkaloid

and RNA, constant but varying their mol fractions from 0 to 1. The difference in fluorescence intensity (ΔF) was plotted against the mol fraction of the alkaloid and the break point corresponds to the intercept between the two slopes. The stoichiometry was derived as [(1-χ_{CHL})/ χ_{CHL}], where χ_{CHL} denotes the mol fraction of CHL. The results reported are averages of three independent experiments.

Fluorescence polarization studies

Fluorescence polarization anisotropy measurements of the (alkaloid + RNA) complexes were carried out as per the procedure of Larsson and colleagues[60] on the Hitachi F4010 spectrofluorimeter.[61] The excitation and emission wavelengths were fixed at 338 and 550 nm, respectively. The excitation and emission slit widths were fixed at 5 nm. Readings were observed 5 min after each addition to ensure stable complex formation. Each reading was an average of four measurements. Anisotropy was calculated using the equation[60]

$$A= (I_{vv} - I_{vh}G) /(I_{vv} + 2I_{vh}G) \quad (4)$$

Here G is the ratio I_{hv}/I_{hh} used for instrumental correction. G is the ratio I_{hv}/I_{hh}. I_{vv}, I_{vh}, I_{hv} and I_{hh} represent the fluorescence signal for excitation and emission with the polarizer positions set at (0^o, 0^o), (0^o, 90^o), (90^o, 0^o) and (90^o, 90^o), respectively.

Fluorescence quenching studies

The anionic quencher I^- was used for quenching experiments. The experiment was performed by mixing, in different ratios, two solutions, one containing KCl, the other containing KI, in the aqueous solution at a fixed total ionic strength. Experiments were performed at a constant P/D (polynucleotide/alkaloid molar ratio) monitoring fluorescence intensity as a function of changing concentration of iodide ions as described previously.[38] The data were plotted as Stern–Volmer plots of relative fluorescence intensity (*Fo*/*F*) versus [I^-].[38]

Viscosity measurements

For viscosity measurements we used a Cannon-Manning Type 75 semi micro capillary viscometer from Cannon Instruments Co. (State College, PA, USA). It was mounted vertically in a constant temperature bath maintained at 20±1°C. Flow times of the complexes (alkaloid + RNA) were measured by an electronic stopwatch model HS-30W (Casio Computer Co. Ltd., Tokyo, Japan) with an accuracy of ±0.01 s.

Measurement of energy transfer measurements

Energy transfer from the RNA helices to the bound alkaloid was measured from the excitation spectra of the complex in the wavelength range 220–310 nm.[47,53] Keeping a fixed emission wavelength of 550 nm the excitation spectra were recorded for CHL. The ratio $Q=q_b/q_f$, where q_b and q_f are the quantum efficiencies of bound and free alkaloid, respectively, were calculated for each wavelength using the equation $Q=q_b/q_f = I_b\varepsilon_f/I_f\ \varepsilon_b$ where I_b and I_f are the fluorescence intensities of the alkaloids in the presence and absence of the RNA helices, respectively, and ε_b and ε_f are the corresponding alkaloid molar absorption coefficients. A plot of the ratio, Q_λ/Q_{310} against wavelength was constructed. The wavelength of 310 nm was chosen as the normalization wavelength due to the negligible absorbance of RNA's at this wavelength.

Ethidium bromide displacement assay

The displacement assay was performed in 50 mM Tris HCl buffer (pH 6.3) with Shimadzu RF-5301PC spectrofluorimeter in fluorescence free quartz cuvettes of 1 cm path length at 20 °C. Excitation and emission slit widths were kept at 5 nm each. CHL was added to a pre-equilibrated mixture of RNA helices (50 μM) and EtBr (7 μM). The fluorescence intensity at 590 nm (λ_{ex} = 490 nm) was recorded upon each addition of CHL. The alkaloid concentration required to

quench the fluorescence of the ethidium–RNA complex by 50% (C_{50}) was derived from a plot of variation of the relative fluorescence intensity at 595 nm versus alkaloid concentration.[62]

Circular dichroism studies

Circular dichroism (CD) spectra were recorded using a PC controlled spectropolarimeter, JASCO J815 unit (Jasco, Hachioji, Japan) equipped with a temperature programmer (model PFD 425L/15) at 20±1°C. A rectangular strain free quartz cuvette of 1 cm path length was used. Each spectrum was averaged from four successive accumulations at a scan rate of 100nm/min. keeping a band width of 1.0 nm at a sensitivity of 100 milli degrees. Base line correction, smoothing and normalization to nucleotide concentration in the region 210–400 nm was performed on each spectra. Fixed amount of the RNA (30 μM) was titrated with increasing concentration of CHL. Each spectrum reported is an average of four runs after complete complex formation. The molar ellipticity values [θ] are expressed in terms of nucleotides.

Optical thermal melting and differential scanning calorimetry studies

Absorbance versus temperature profiles (optical thermal melting profiles) of the RNA helices and RNA-alkaloid complexes were measured on the Shimadzu Pharmaspec 1700 unit equipped with a peltier-controlled TMSPC-8 model accessory (Shimadzu Corporation) as described earlier.[63] In a typical experiment, the triplex sample (~40 μM) and double stranded sample (~30 μM) were mixed with the varying concentration of the alkaloid under study in the desired degassed buffer into the eight-cell micro-optical cuvette of 1 cm path length, and the temperature of the microcell accessory was raised at a heating rate of 0.5°C/min while continuously monitoring the absorbance change at 260 nm. The thermal melting temperature (T_m) was taken as the midpoint of the melting transition as determined by the maxima of the first derivative plot.

Differential scanning calorimetry (DSC) was performed on an ultrasensitive VP DSC micro calorimeter (MicroCal LLC, Northampton, MA, USA) as described previously.[63,64] The samples were incubated at 20 ^{o}C for 10 min. and scanned from 20 ^{o}C to 90 ^{o}C at approximately 25 psi pressure. Prior to sample scans, the instrument was thermally stabilized by repeated buffer scans under identical scan rate and in the same temperature range. 50 μM of the polynucleotide solution was scanned to obtain the melting profile of the free form. Thereafter, the RNA solution was incubated with different concentrations of CHL for 10 min. to ensure complete complexation and scanned to obtain the DSC profile of the bound form. The thermograms were analyzed using the in-built VP Viewer with Origin 7.0 software. The non-2-state (cursor initiation) model of curve fitting was employed to fit the raw DSC thermograms.

Isothermal titration calorimetry (ITC)

The detailed calorimetric studies were done on a MicroCal VP ITC calorimeter (MicroCal LLC) at 20 °C using protocols developed in our laboratory and described previously in details.[39,40,65] Briefly, 10 μL aliquots of RNA solution were injected from a 299 μL rotating syringe (290 rpm) into the sample cell containing 1.4235 mL of the alkaloid solution. Corresponding control experiments to determine the heat of dilution of the RNA to buffer were performed by injecting identical volumes of the same concentration of the RNA into buffer. Each injection generated a heat burst curve (micro calories per second versus time). The area under each peak was determined by integration using Origin software to give a measure of heat associated with the injection. Subtraction of the control heat from the corresponding heat of RNA-alkaloid reaction gave the heat of alkaloid-RNA binding. The heat of buffer-alkaloid mixing was found to be negligible. The injection heats were plotted as a function of the molar ratio and fit with a model of one site binding site and analyzed to estimate the binding affinity (K_a), the binding

stoichiometry (N), and the enthalpy of binding (ΔH^o). The binding Gibbs energy (ΔG^o) and the entropic contribution ($T\Delta S^o$) to the binding were subsequently calculated from standard relationships.[66,67]

Acknowledgements

Financial support for this work was provided from the network project 'GenCODE' (BSC0123) of the Council of Scientific and Industrial Research (CSIR), Govt. of India, P. Basu is a NET-Senior Research Fellow of the University Grants Commission, Govt. of India. Authors thank all the colleagues of the Biophysical Chemistry Laboratory for their help and cooperation at every stage of this investigation.

Supplementary data

Supplementary data associated with this article can be found, in the online version, at …..

References

1 S. Geisler and J. Coller, *Nat. Rev. Mol. Cell Bio.*, 2013, **14**, 699-712.

2 A. C. Cheng, V. Calabro and A. D. Frankel, *Curr. Opin. Struct. Biol.*, 2001, **11**, 478–484.

3 T. Hermann, *Biochimie*, 2002, **84**, 869–875.

4 Q. Vicens and E. Westhof, *Chembiochem*, 2003, **4**, 1018–1023.

5 C. V. Catapano, E. M. McGuffie, D. Pacheco and G. M. Carbone, *Biochemistry*, 2000, **39**, 5126–5138.

6 M. Faria, C. D. Wood, L. Perrouault, J. S. Nelson, A. Winter, M. R. H. White, C. He´le`ne and C. Giovannangeli, *Proc. Natl. Acad. Sci. USA*, 2000, **97**, 3862–3867.

7 Z. Luo, M. A. Macris, A. F. Faruqi and P. M. Glazer, *Proc. Natl. Acad. Sci. USA*, 2000, **97**, 9003–9008.

8 J. Song, Z. Intody, M. Li and J. H. Wilson, *Gene*, 2004, **324**, 183–190.

9 B. P. Belotserkovskii, E. De Silva, S. Tornaletti, G. Wang, K. M. Vasquez and PC Hanawalt, *J. Biol. Chem.*, 2007, **282**, 32433–32441.

10 C. Giovannangeli and C. He´le`ne, *Nat. Biotechnol.*, 2000, **18,** 1245–1246**.**

11 T. Povsic, S. A. Strobel and P. B. Dervan, *J. Am. Chem. Soc.*, 1992, **114**, 5934–5941.

12 K. M. Vasquez, L. Narayanan and P. M. Glazer, *Science*, 2000, **290**, 530–533.

13 M. R. Rajeswari, *J. Biosci.*, 2012, **37**, 519–532.

14 F. A. Buske, J. S. Mattick and T. L. Bailey, *RNA Biol.*, 2011, **8**, 427–439.

15 G. Devi,Y. Zhou, Z. Zhong, D-F. K. Toh and G. Chen, *WIREs RNA*, 2015, **6**, 111–128.

16 A. Jain, A. Bacolla, P. Chakraborty, F. Grosse and K. M. Vasquez, *Biochemistry*, 2010, **49**, 6992–6999.

17 G. Shafi, K. Jamil, A. Kapley, H. J. Purohit and M. C. Vamsy, *Biotechnol. Mol. Biol. Rev.*, 2008, **4**, 55–70.

18 P. A. Sharp, *Genes Dev.*, 1999, **13**, 139–141.

19 P. K. Gupta, *Imaging Microscopy*, 2006, **8**, 14–6.

20 B. N. Kalali, G. Ko¨ llisch, J. Mages, T. Mu¨ ller, S. Bauer, H. Wagner, J. Ring, R. Lang, M. Mempel and M. Ollert, *J. Immunol.*, 2008, **181**, 2694–2704.

21 G. Meister and T. Tuschl, *Nature*, 2004, **431,** 343–349.

22 S. Kumar, P. Deepak, S. Kumar, P. K. Gautam and A. Acharya, *J. Cancer Res. Ther*., 2013, **9,** 693–700.

23 S. Gibbons, J. Leimkugel, M. Oluwatuyi and M. Heinrich, *Phytother. Res.*, 2003, **17**, 274–275.

24 J. M. Herbert, J. M. Augereau, J. Gleye and J. P. Maffrand, *Biochem. Biophys. Res. Commun.*, 1990, **172,** 993–999.

25 R. Yu, S. Mandlekar, T. H. Tan and A. N. Kong, *J. Biol. Chem.*, 2000, **275,** 9612–9619.

26 S. J. Chmura, M. E. Dolan, A. Cha, H. J. Mauceri, D.W. Kufe and R.R. Weichselbaum, *Clin. Cancer Res.*, 2000, **6,** 737–742.

27 S. Yamamoto, K. Seta, C. Morisco, S. F. Vatner and J. Sadoshima, *J. Mol. Cell. Cardiol.*, 2001, **33,** 1829–1848.

28 J. O'Neill, M. Manion, P. Schwartz and D. M. Hockenbery, *Biochim. Biophys. Acta*, 2004, **1705,** 43–51.

29 Z. F. Zhang, Y. Guo, J. B. Zhang and X. H. Wei, *Arch. Pharm. Res.*, 2011, **34**, 791–800.

30 Z. Yu, R. M. Schmaltz, T. C. Bozeman, R. Paul, M. J. Rishel, K. S. Tsosie and S. M. Hecht, *J. Am. Chem. Soc.*, 2013, **135,** 2883−2886.

31 B. R. Schroeder, M. I. Ghare, C. Bhattacharya, R. Paul, Z. Yu, P. A. Zaleski, T. C. Bozeman, M. J. Rishel and S. M. Hecht, *J. Am. Chem. Soc.*, 2014, **136**, 13641−13656.

32 P. Basu, D. Bhowmik and G. Suresh Kumar, *J. Photochem. Photobiol. B*, 2013, **129**, 57-68.

33 P. Basu and G. Suresh Kumar, *J. Photochem. Photobiol. B*, 2014, **138**, 282-294.

34 M. Ferraroni, C. Bazzicalupi, P. Gratteri and A. R. Bilia, PDB ID: 4D9Y.

35 L. P. Bai, M. Hagihara, K. Nakatani and Z. H. Jiang, *Sci. Rep.*,2014, **4,** 6767.

36 A. B. Pradhan, L. Haque, S. Bhuiya and S. Das, *RSC Adv.*, 2014, **4**, 52815–52824.

37 S. Das, G. Suresh Kumar, A. Ray and M. Maiti, *J. Biomol. Struct. Dyn.*, 2003, **20,** 703-713.

38 A. Ray, G. Suresh Kumar, S. Das and M. Maiti, *Biochemistry*, 1999, **38,** 6239-6247.

39 M. M. Islam, S. Roy Chowdhury and G. Suresh Kumar, *J. Phys. Chem. B*, 2009, **113,** 1210–1224.

40 S. Roy Chowdhury, M. M. Islam and G. Suresh Kumar, *Mol. BioSyst.*, 2010, **6**, 1265–1276**.**

41 J. D. McGhee and P. H. von Hippel, *J. Mol. Biol.*, 1974, **86**, 469–489.

42 R. Sinha and G. Suresh Kumar, *J. Phys. Chem. B*, 2009, **113**, 13410–13420.

43 V. A. Bloomfield, D. M. Crothers, and I. Tinoco, Jr., *Phys. Chem. Nucleic Acids*, 1974. 442-443,

44 P. V. Scaria and R. H. Shafer, *J. Biol. Chem.*, 1991, **266**, 5417-5423.

45 J. B. Le Pecq and C. Paoletti, *J. Mol. Biol.*, 1967, **27,** 87-106.

46 C. G. Reinhardt, B. P. Roques and J. B. Le Pecq, *Biochem. Biophys. Res. Commun.*, 1982, **104**, 1376-1385.

47 M. A. Sari, J. P. Battioni, D. Dupre, D. Mansuy and J. B. Le Pecq, *Biochemistry*, 1990, **29**, 4205-4215.

48 D. E. Graves and L. M. Velea, *Curr. Org. Chem.*, 2000, **4**, 915–929.

49 A. L. Faig, *Biopolymers*, 2007, **87**, 293–301.

50 N. J. Buurma and I. Haq, *Methods*, 2007, **42,** 162–172**.**

51 J. B. Chaires, *Arch. Biochem. Biophys.*, 2006, **453,** 26–31.

52 A. Basu, P. Jaisankar and G. Suresh Kumar, *Mol. Biol. Rep.*, 2014, **41**, 5473–5483.

53 D. Bhowmik, S. Das, M. Hossain, L. Haq and G. Suresh Kumar, *Plos One*, 2012, **7**, e37939.

54 A. Basu, P. Jaisankar and G. Suresh Kumar, *Bioorg. Med. Chem.*, 2012, **20**, 2498–2505.

55 H. Absolinova, L. Jancˇarˇ, I. Jancˇarˇova, J. Vicˇar and V. Kubanˇ, *Cent. Eur. J. Chem*., 2010, **8**, 626–632.

56 K. Bhadra, M. Maiti and G. Suresh Kumar, *Biochim. Biophys. Acta*, 2007, **1770**, 1071–1080.

57 P. Basu and G. Suresh Kumar, *J. Chem. Thermodyn*., 2015, **81**, 116-123.

58 M. Hossain, A. Kabir and G. Suresh Kumar, *J. Biomol. Struct. Dyn.,* 2012, **30**, 223–234.

59 P. Giri and G. Suresh Kumar, *Arch. Biochem. Biophys.,* 2008, **474**, 183–192.

60 A. Larsson, C. Carlsson, M. Jonsson and B. Albinsson, *J. Am. Chem. Soc.,* 1994, **116**, 8459–8465.

61 R. Sinha, M. M. Islam, K. Bhadra and G. Suresh Kumar, *Bioorg. Med. Chem.,* 2006, **14**, 800–814.

62 J. H. Tan, Y. J. Lu, Z. S. Huang, L. Q. Gu and J. Y. Wu, *Eur. J. Med. Chem.,* 2007, **42**, 1169–1175.

63 M. M. Islam, R. Sinha and G. Suresh Kumar, *Biophys. Chem*., 2007, **125**, 508–520.

64 P. Paul and G. Suresh Kumar, *J. Chem. Thermodyn.*, 2013, **64**, 50–57.

65 J. Bhattacharyya, A. Basu and G. Suresh Kumar, *J. Chem. Thermodyn.*, 2014, **75**, 45–51.

66 R. Sinha, M. Hossain and G. Suresh Kumar, *Biochim. Biophys. Acta*, 2007, **1770**, 1636-1650.

67 R. Sinha, M. Hossain and G. Suresh Kumar, *DNA Cell Biol.,* 2009, **28**, 209-219.